Women's view on fasting during labor in a tertiary care obstetric unit. A prospective cohort study

Lionel Bouvet, Julie Garrigue, François-Pierrick Desgranges, Federica Piana, Géry Lamblin, Dominique Chassard

Version of Record: https://www.sciencedirect.com/science/article/pii/S0301211520304838
Manuscript_1674022d43c9ec5d076ca5a356d15923

Predicting final stage sintering grain growth affected by porosity

Gabriel Kerbart[1], Charles Manière[1], Christelle Harnois[1], Sylvain Marinel[1]

1 Normandie Univ, ENSICAEN, UNICAEN, CNRS, CRISMAT, 14000 Caen, France

Abstract

Grain growth has a definitive impact on the quality of transparent sintered materials in areas such as ballistics, biomaterials, jewelry, etc. Controlling the sintering trajectory at the precise moment of final stage sintering is one of the main sintering challenges for obtaining high-performance, fully-dense nano-ceramics. However, the final stage of sintering involves a very complex coupling between the rate of porosity elimination/grain growth and transition mechanisms. This complexity makes predicting the sintering trajectory very difficult, and most transparent material production escapes this problem by using expensive high-pressure methods such as hot isostatic pressing (HIP). In the quest for a pressureless transparent material process, this paper addresses the challenge of predicting grain growth in the transition domain from the grain growth onset (in a high porosity region) to full density for $MgAl_2O_4$ spinel. We present a comprehensive modeling approach linking theoretical models such as Zhao & Harmer's and Olevsky's equations to accurately predict the complex grain growth transition region of final stage sintering. This modeling approach opens up the possibility for numerical exploration of microstructure development via underlying kinetics experimental identification.

Keywords:
Grain growth; Sintering; Microstructure development; $MgAl_2O_4$; Mechanisms; Modeling

Nomenclature

θ Porosity
θ_c Critical porosity
$\dot{\theta}$ Porosity elimination rate (s^{-1})
N_g Mean number of pore per grain
n, m Grain growth equation exponents
α Surface energy ($J.m^{-2}$)
R Gas constant 8.314 ($J.mol^{-1}.K^{-1}$)
T Temperature (K)
$\dot{G}$ Grain growth rate ($m.s^{-1}$)
G Grain size (m)
G_0 Initial grain size (m)
p Grain growth equation grain size exponent
K Grain growth factor ($m^{1+p}.s^{-1}$)
k_0 Grain growth pre-exponential factor ($m^{1+p}.s^{-1}$)
Q Grain growth activation energy ($J.mol^{-1}$)
t Time (s)

K' Constant for isothermal condition ($m^{1+p}.s^{-1}$)
C, A Constants
a, b, c fitting constants
w The sintering equation grain size exponent
D The diffusion coefficient
k The Boltzmann constant (1.38064852E-23 $J.K^{-1}$)

I. Introduction

The scientific community and industry takes much interest in the development of transparent polycrystalline ceramic technology due to their numerous applications for jewelry, laser hosts, spacecrafts and IR windows for military applications[1]. Ceramics' main attractive features are their thermo-mechanical properties, fracture toughness, and high hardness from room temperature to high temperatures (>1000°C). For some of them, their intrinsic transparency in the visible-IR range and their low cost of raw materials [2] also enhance their attractiveness. Several ceramic compositions present advantageous mechanical properties along with transparency, including alumina Al_2O_3, aluminum oxynitride spinel $Al_{23}O_{27}N_5$ and magnesium aluminate spinel $MgAl_2O_4$ [1]. Compared to alumina, which is known for its transparency and better mechanical properties, $MgAl_2O_4$ does not exhibit birefringence properties. This birefringence has an impact on transparency and implies a minimal grain size (<400 nm for alumina) in order to avoid the degradation of optical properties. Moreover, transparency can only be achieved for highly pure and fully dense materials. In the case of magnesium aluminate spinel ($MgAl_2O_4$), hereafter termed spinel, these applications also require minimal grain growth to optimize mechanical properties [3,4]. The impact of grain size on the mechanical properties of spinel is well documented. It's known that for this type of ceramic material, smaller grain size improves mechanical properties due to its Hall-Petch tendency [5].

The latest methods for sintering $MgAl_2O_4$ include Hot Isostatic Pressure (HIP) and Spark Plasma Sintering (SPS) [6–10]. These sintering methods limit grain growth through the application of mechanical pressure (gas pressure for HIP and uniaxial mechanical pressure for SPS). The best result for HIP sintering of spinel has been obtained with pretreatment, such as conventional sintering [6,7]. A pre-sintering stage followed by a HIP treatment at 1400°C leads to a transparent spinel with a grain size of 400-600 nm [6]. Similarly, Goldstein *et al* [8] obtained equivalent grain size with cold-isostatic pressing, conventional pre-sintering and HIP sintering at 1320°C-170MPa. Transparent spinel has also been obtained using SPS sintering by Bonnefont *et al* [9] who reported a grain size of 275 nm, at 1300°C-72 MPa. Sokol *et al* [10] obtained nano-sized grains of transparent spinel with a mean grain size of 50 nm by HPSPS (High Pressure Spark Plasma Sintering) at 1000MPa and 1000°C. However, those methods involve pressure and specific atmospheric conditions during sintering (argon pressure or vacuum with graphite contact, for respectively HIP and SPS). For SPS, graphite pollution has been widely reported to be a limiting transparency phenomenon [11,12]. Dopants were also studied for the sintering of spinel, notably LiF [13–15]. However, this sintering aid seems to initiate exaggerated grain growth for sintering temperature around 1620-1650°C [16].

The study's objective is to model the spinel grain growth during sintering. This modeling will be useful for predicting the sintering trajectory and therefore for finding optimized thermal treatment cycles [17]. Sintering trajectory models have proven to be a powerful tool for obtaining nano-grain, fully-dense "Zpex" grade Tosoh zirconia [18]. In this approach, the sintering response is modeled *via* a combination of densification and the grain growth model. Indeed, in addition to the detrimental

effect on the ceramic 's mechanical properties, grain growth slows down the sintering kinetic by extending the diffusion path [19–21]. This effect is very active in the final stage of sintering and was used to correct the sintering model densification curve at the end of sintering [22,23]. In the well-known equation (1) below, which originated from the analytical form of various solid-state pressureless sintering mechanisms [24], the final stage effect takes his origin in the term G^w which divides the porosity elimination rate [19].

$$\dot{\theta} = \frac{-C\, f(\theta)\alpha D}{G^w kT} \qquad (1)$$

In this formula, the grain size exponent *w* is 3 for lattice diffusion and 4 for grain boundary diffusion [19]. Equation (1) is the base of numerous sintering methods for studying sintering mechanisms, such as master sintering curves [25], kinetic fields and the Wang and Raj approach [26], etc.

The same approach is applied to a spinel powder for controlling the sintering trajectory. We concentrate our efforts on the temperature onset region of the final sintering stage where the grain growth takes place. This transition region, where both densification and grain growth are active, represents the best opportunity for sintering optimization [27,28]. The difficulty and the interesting aspect of identifying grain growth behavior in this region lies in the influence of porosity on grain growth. At low temperatures, the grain growth kinetic is slow due to the pinning effect of the porosity located on the grain boundaries. After the separation of pores from the grain boundaries at higher temperatures, the grain growth kinetic accelerates [18]. This separation has been studied by numerous authors [29–31] and is known to be a key aspect of sintering, particularly with respect to obtaining transparent ceramics. In order to model the grain growth in this interesting transition region, we will consider the two grain growth models from Zhao and Olevsky which take into account the porosity contribution. Zhao and Harmer published a three-part study [32–34] where the grain growth is modeled theoretically via a model which takes into account porosity and pore size distribution. In the Olevsky et al model [35], porosity is implemented via a function which includes a critical porosity and easily models the transition between the region of porosity influence and the traditional form of grain growth for fully-dense materials at high temperatures.

In this work, we will compare these two models and identify the grain growth of spinel at different temperatures in the transition region where grain growth is active. Special attention will be paid to the description of the evolution of the grain growth mechanisms in the transition region.

II. Theory and calculation

II.1. Theoretical model of grain growth with porosity

The traditional grain growth model based on grain boundary mobility (with or without pores) obeys the following relation of the grain growth rate [19,36,37]:

$$\dot{\mathrm{G}} = \frac{K(T)}{G^p} \qquad (2)$$

with K(T) defined by various parameters that can be expressed by an Arrhenius relation:

$$K(T) = K_0\, exp\left(\frac{-Q}{RT}\right) \quad (3)$$

For sintering, the equation (2) is often known by its integration form $G^{p+1} = G_0^{p+1} + K't$ for fully dense or porous specimens and for isothermal conditions (K' constant)[38,39]. For anisothermal conditions, the term $K't$ of the integration form is replaced (mathematically) by $A\int_{t0}^{t} exp\left(\frac{-Q}{RT}\right) dt$ in order to take into account the thermal history of $K(T)$ as in the equivalent rate formulation (2) [19]. The exponent of the integrated form (*p+1* between 2 and 4) can be related to various grain growth mechanisms such as: 4 for pore control by surface diffusion, 3 for pore control by lattice diffusion or 2 for boundary control of pure system or evaporation/condensation pore drag[40]. There are numerous grain growth mechanisms and exponents but, as highlighted by Rahaman, the experimental exponent value during sintering is often close to 3 and may also evolve with temperature and additional factors such as the impurity segregation [19]. Similarly, a transition of the grain growth kinetic is often observed with temperatures corresponding to a change in the grain growth regime [18,41]. This change has supposedly been linked to a change in the pore drag regime on grain growth. In the present approach, we will investigate the impact of both the porosity and the change of the grain growth mechanism during the sintering of spinel.

The impact of the porosity on the grain growth kinetic is mainly investigated by various identified mechanisms [40] using equation (2). However, the evolution of the porosity elimination may directly impact the grain growth kinetic regardless of the exponent. Very few theoretical studies have been published in this regard [21], but one can cite the works of Zhao and Harmer [32–34]. One of their main achievements is the grain growth equation depending on the porosity θ and the mean number of pores per grains N_g:

$$\dot{\mathrm{G}} = \frac{K(T)}{G^p}\left(\frac{N_g^m}{\theta^n}\right) \quad (4)$$

With p, n and m, exponents depend on the control mechanisms (Surface diffusion: *p=3, n=4/3 and m=1/3*, lattice diffusion: *p=2, n=1 and m=0*). Riedel and Svoboda propose various grain growth models with a similar form [42]. Olevsky's grain growth model corrected the traditional theory by modeling the effect of porosity on grain growth *via* a critical porosity function:

$$\dot{\mathrm{G}} = \frac{K(T)}{G^p}\left(\frac{\theta_c}{\theta + \theta_c}\right)^n \quad (5)$$

These equations modulate grain growth by the introduction of a porosity influence function which reduces the grain growth kinetics for various porosity levels. However, when samples approach maximum density, Zhao's function of porosity tends toward infinity while Olevsky's empirical function tends toward 1, which reduces the model to its conventional form for normal grain growth in fully-dense materials.

Zhao and Harmer use equation (4) in combination with a densification model to model the sintering trajectory. However the consequence of the grain growth function singularity for full density makes the grain growth rate tend toward infinity close to full densification ($1/\theta^n \rightarrow \infty$). Furthermore, the determination of the mean number of pores per grain (*Ng*) is very difficult for

classical microstructures with a high variety of pores. For this reason, Zhao and Harmer used the pore former to ease the experimental identification of *Ng*. Therefore, Olevsky's model appears to be more suitable for routine experimental use. However, it's important to understand if this empirical function describes the grain growth mechanism in the same way as the theoretical equations (like those of Zhao and Harmer) do.

In order to compare Olevsky and Zhao's and Harmer's grain growth law porosity function, the experimental results of Zhao and Harmer's function (N_g^m/θ^n) were plotted in Fig. 1 for a *p* exponent of 2 and 3, corresponding respectively to surface and lattice diffusion pore control mechanisms [34]. Olevsky's function[35] in the form $a(\frac{\theta_c}{\theta+\theta_c})^n$ was also plotted in Fig. 1, with a fitting parameter "*a*" that can be assumed to be taken from the term K(T) in equation (5). It's clearly demonstrated in Fig. 1 that Olevsky's empirical critical porosity function has the same tendency of Zhao and Harmer's grain growth model. Nevertheless, compared to the latter, Olevsky's function depends only on the porosity and does not suffer from the singularity for full densification case (due to the critical porosity term). Based on these results, the following study will consider Olevsky's function to estimate the porosity influence on the grain growth of spinel. It will be demonstrated that this porosity function is inevitable for describing grain growth behavior in the transition region mentioned in the introduction.

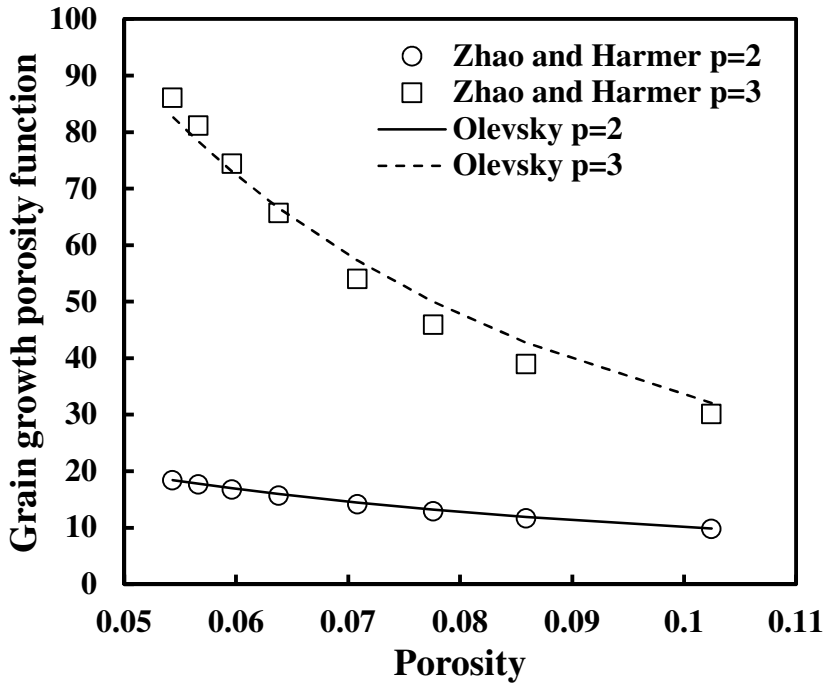

Figure 1 Zhao and Harmer's theoretical grain growth porosity dependent term fitted by Olevsky's empirical function

II.2. Identification methodology

In order to identify the parameters of the grain growth model, four main steps are required and are defined below. This methodology is based on interrupted isothermal sintering tests at various temperatures and a double regression for determining the grain growth kinetics (see method scheme in Fig. 2).

Fig. 1 Study flow

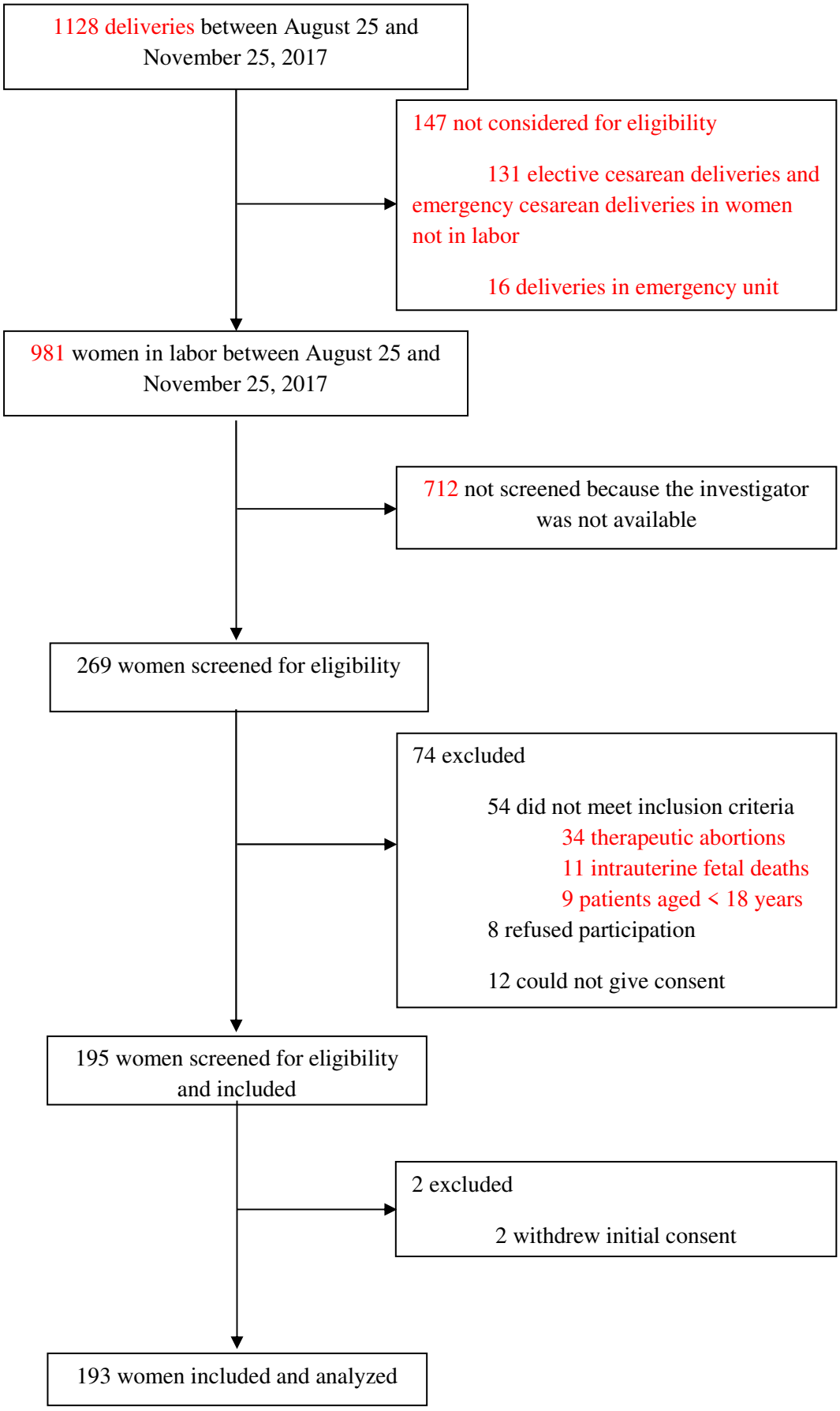

Fig. 2. Thirst (A) and hunger (B) related discomfort score according to whether women did have or not oral intake during labor. Vertical bars denote interquartile ranges. *p < 0.0001 compared to hunger-related discomfort score within each group. Score ≥ 4 (dotted line) corresponds to significant level of discomfort.

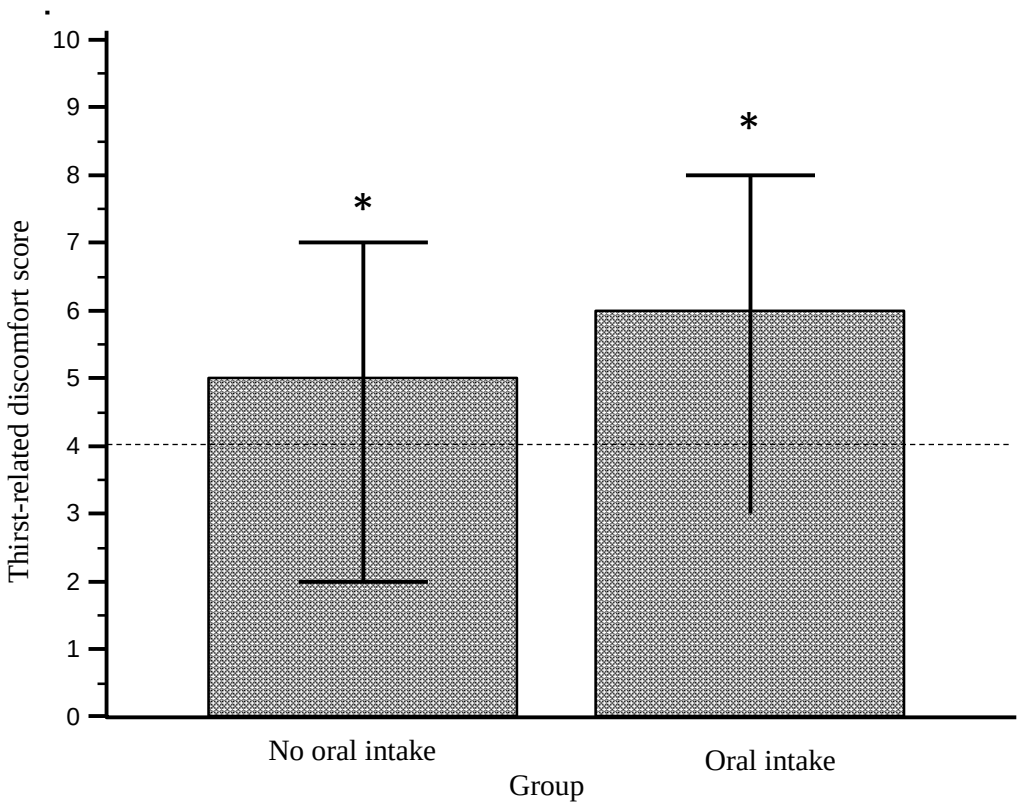

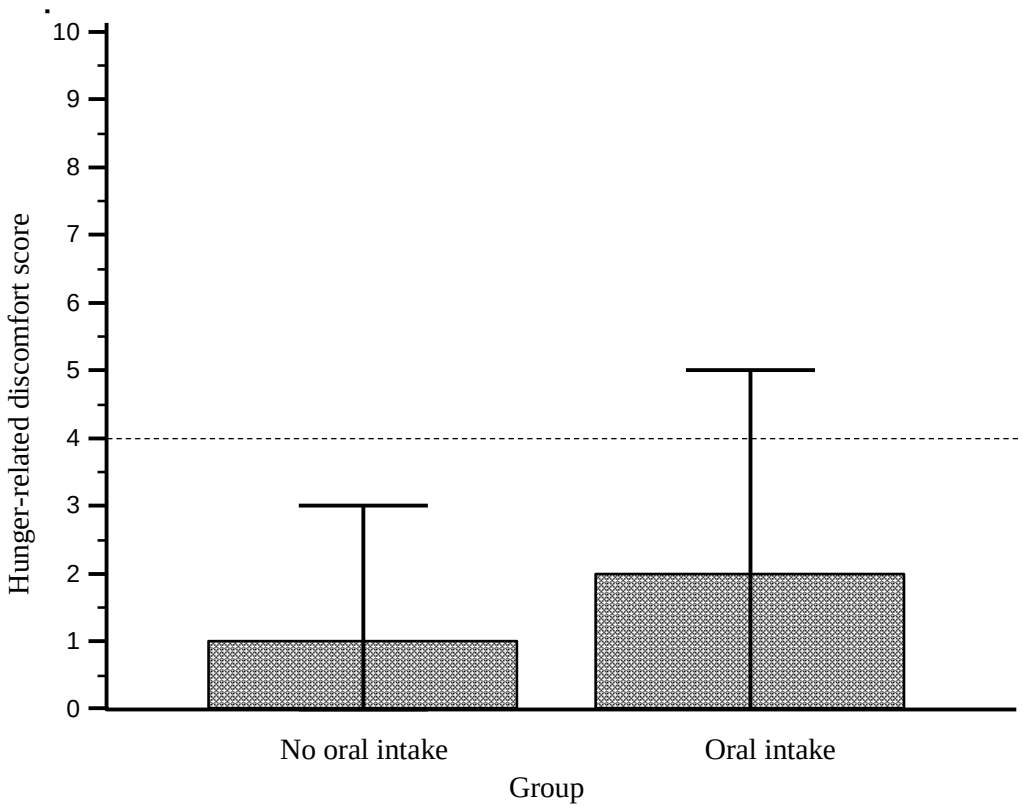

Table 1

Patient characteristics**.**

	N = 193
Age (year)	30 [26-34]
Weight (kg)	75 (13)
Height (cm)	165 (6)
Body mass index (kg/m^2)	27 [25-30]
Parity	
0	94 (49%)
1	59 (31%)
≥2	40 (20%)
Gravidity	
1	78 (40%)
2	53 (28%)
≥3	62 (32%)
ASA physical status	
1	165 (86%)
2	27 (14%)
3	1 (1%)
Mallampati grade	
1	114 (59%)
2	55 (29%)
3 and 4	24 (12%)
Medical history	
Gastro-esophageal reflux	79 (41%)
Hiatal hernia	2 (1%)
Gastric band	2 (1%)
Pregnancy data	
Single pregnancy	190 (98%)
Gestational diabetes	27 (14%)
Fetal macrosomia	16 (8%)
Uterine scars	13 (7%)
Preeclampsia	1 (1%)

Data are expressed as median [interquartile range], mean (standard deviation) or n (%). ASA: American Society of Anesthesiologists.

Table 2

Delivery and anesthesia data.

Characteristics of delivery and anesthesia	N = 193
Gestational age at arrival in the delivery room (days)	281 [275-286]
Cervix dilation at arrival in the delivery room (cm)	3 [3-4]
Mode of analgesia	
Epidural analgesia	176 (92%)
None	16 (8%)
Intravenous patient controlled analgesia with opioids	1 (0.5%)
Progress of labor	
Spontaneous onset of labor	156 (81%)
Oxytocine augmentation of labor	77 (40%)
Induced onset of labor	37 (19%)
Non-reassuring fetal status	65 (34%)
STAN monitoring required	26 (14%)
Labor duration (hours)	6.5 [3.9-8.7]
Mode of delivery	
Vaginal delivery	181 (94%)
Vaginal intrumental delivery	30 (16%)
Cesarean section in the course of labor	12 (6%)
Overall pain score during labor (cm)	3 [1-4]
Volume of intravenous hydration (ml)	500 [500-1000]

Data are expressed as median [interquartile range] or n (%). STAN: fetal electrocardiogram ST segment analysis.

Table 3

Main characteristics of women according to whether or not they did drink or eat during labor.

	Oral intake n = 119	No oral intake n = 74	p value
Cervix dilation at arrival in the delivery room (cm)	3 [3-4]	4 [2-5]	0.06
Gestational age at arrival in the delivery room (days)	282 [276-287]	278 [274-285]	0.03
Duration of labor (hours)	7.7 [5.6-10.4]	6.2 [4.5-8.2]	0.11
ASA physical status = 1	103 (87%)	62 (84%)	0.68
Mallampati grade ≤ 2	105 (88%)	64 (86%)	0.82
Body mass index ($kg.m^{-2}$)	27 [25-30]	27 [24-30]	0.80
Gastro-esophageal reflux	43 (36%)	36 (49%)	0.12
Single pregnancy	117 (98%)	73 (99%)	0.68
Gestational diabetes	18 (15%)	9 (12%)	0.72
Spontaneous induction of labor	92 (77%)	64 (86%)	0.17
Oxytocin augmentation of labor	54 (45%)	23 (31%)	0.051
Epidural analgesia	115 (97%)	61 (82%)	0.001
Non reassuring fetal status	42 (35%)	23 (31%)	0.66
STAN monitoring	18 (15%)	8 (11%)	0.52

Data are expressed as median [interquartile range] or n (%). ASA: American Society of Anesthesiologists. STAN: fetal electrocardiogram ST segment analysis.